An internal variable model for plastic remodeling in fibrous materials

Antonino Favata, Andrea Rodella, Stefano Vidoli

Department of Structural and Geotechnical Engineering
Sapienza University of Rome, Rome, Italy
antonino.favata@uniroma1.it
andrea.rodella@uniroma1.it
stefano.vidoli@uniroma1.it

Abstract

We propose a continuum model of fibrous materials that may undergo an internal reorganization, which turns out in a plastic change of the orientation of the fibers, if a threshold is achieved. We find that the remodeling may induce a rich material response. In a traction test, when the threshold condition is reached, we show that the most general transversely isotropic material may evolve in three different ways; in particular, the fibers asymptotically tend (regularly or with jumps): (A) to a given angle; (B) to align perpendicularly with respect to the load direction; (C) to align with the load direction if their initial angle is less than a given value, or perpendicularly, otherwise. We provide analytical solutions for the evolutive homogeneous problem and some numerical results for a non-homogeneous condition. The theory is very general and can find applications in several problems arising in material mechanics.

Keywords: Fibrous materials, remodeling, plasticity, phase field

1. Introduction

Fibrous materials have recently gained an increasing interest for their preeminent role both in biology and in the design of engineered materials, often bio-inspired. Almost all tissues and organs of the human body are organized in fibrous structures, as in skin, cartilage, connective tissues, collagen, all endowed with nano-/microsized fibers. On the other hand, a variety of applications of engineered fibrous materials is growing up, such as textiles, nonwovens, composites. The literature in the subject is huge and spans several different fields; see [37, 6, 48, 2, 26], to mention a few.

Often fibrous materials may undergo a plastic reorganization, which turns out in a change of the orientation of the fibers. This is a peculiar behavior of many biological tissues, which drive reorientation by external stimuli at chemo-mechanical levels [15, 30, 16, 31, 32, 3, 28, 45, 43, 12, 33]. Their behavior is characterized by both elastic [18, 14] and inelastic [9, 8, 4] mechanical properties. In particular, the extracellular matrix may undergo to a plastic remodeling, leading to irreversible deformations; such a behavior affects cell spreading, motility, and differentiation: *e.g.*, the fibers reorient and guide

the migration of normal and cancer cells. Several studies report this plastic behavior in fibrous matrices after removing external physical forces [49, 4, 7].

Reorientation may also occur in other materials such as liquid crystals, nematic or magneto-rheological elastomers, etc. In particular, in liquid crystals the reorientation can be controlled by magnetic or electric fields [19, 13]. The seminal paper [35] deals with nematic liquid single crystal elastomers (LSCE), and the strain-induced director reorientation process is reported for the case of an arbitrary angle between the original director and the external stress axis. LSCEs show a reorientation of the director, similarly to the well known Frederiks-transition where a director reorientation is induced by electric or magnetic fields. In [36] it is reported that, after a threshold strain, stripe-domains are formed parallel to the external stress with alternating sense of rotation in each domain.

Adaptive structural reorientation is preeminent in many other natural materials, which can be studied to get valuable inspiration to design engineered materials with peculiar properties on demand [39]. For example, although strong interfaces are usually required in man-made composites, relatively compliant and weak interfaces are often preferred in biological materials for easy interfacial mobility [5, 22, 47, 17]. Several mechanisms can be detected in natural materials playing a crucial role in the deformation of the composite, such as the breakage and reformation of sacrificial bonds and the unfolding and refolding of hidden lengths; this yields the matrix a high capability to deform, both elastically and plastically [34, 38, 20]. These mechanisms allow the reinforcement to reorient within the matrix in response to external loads. For example the microfibril angle, *i.e.*, the tilt angle of the cellulose fibrils relative to the longitudinal axis in the one of the major parts of the wood cell wall, the S2 layer, decreases by more than 10° in the *Picea abies* [34]; in the scales of *Arapaima gigas* fish the mineralized collagen fibrils can reorient towards the tensile axis by an average of 6-8° upon loading [50].

The effects of reorientation, in particular those occurring during the post-yield deformation, remain largely unexplored in both biological and man-made composites. Here we focus on the mechanism of a plastic threshold. For sake of simplicity, we neglect other possible relevant physical properties, such as viscous effects; indeed, the asymptotic behavior basically depends on the free energy. Moreover, we focus in particular to 2D problems, since in this context it is possible to obtain analytical solutions.

A word of caution about the title is needed. With *plastic remodeling* we mean a phenomenon that refers to a reorientation of the fibers, representing the microstructure of a continuous medium; this reorientation exhibits two basic characters: (i) a threshold that defines the end of a reversible behavior (what is commonly referred to as "elastic") ; (ii) a permanent change of the microstructure, accompanied by dissipation. In our model there is not any plastic deformation, in the usual sense. There are rather inelastic effects, in the sense that there is something else, besides the elastic strain, that determines the local state; the way we chose to represent these effects is through an *internal variable*, that represents the fiber rotation. This is formally similar to classical plasticity, where the internal variable is given by the plastic strain; but, at variance with classical plasticity, in our model there is not any decomposition of the total (visible) strain. Needless to say, the presence of this additional variable requires an additional constitutive equation, reflecting the hypothesis that, if the local state that determines the stress and the energy is defined by the elastic strain and the rotation, the rate of evolution of the internal variable is also determined by the local state itself. The *elastic range* can be expressed either in terms of a threshold value of the remodeling torque (power-conjugated with

the rate of rotation) or of the elastic strain, being the set of strains for which the fiber direction cannot evolve.

Our model is based on the formulation of continuum mechanics for materials with an internal state variable [11, 23, 29, 24, 25], *i.e.*, the rotation of the fiber. We find that the remodeling may induce, in principle, different material responses. In a traction problem, we show that the most general transversely isotropic material may evolve in three different ways, when the threshold is achieved; in particular, the fibers asymptotically tend (regularly or with jumps): (A) to a given angle; (B) to align perpendicularly with respect to the load direction; (C) to align with the load direction if their initial angle is less than a given value, or perpendicularly, otherwise. Moreover, since the plastic remodeling changes the material response, we find that, in principle, it is possible to have a transition from auxetic to non-auxetic materials: this can happen because a virgin material with a distribution of fibers having a given angle, if sufficiently deformed, changes permanently the orientation, which turns out in a different global response.

The paper is organized as follows. In Sec. 2 we formulate the model of plastic reorientation; in particular, we describe a general process, the dissipation, the yield function. In Sec. 3 we propose a simple but general free energy and provide an analytical characterization of the elastic range. In Sec. 4 we consider a traction problem; we first analytically solve the homogeneous case and carefully describe the rich scenario that reorientation may produce; we then propose numerical solutions for a non-homogeneous problem. Conclusions and further directions of work are finally discussed in Sec. 5.

2. Plastic remodeling

We confine our analysis to a two-dimensional body $\mathcal{B}$. For convenience, we introduce a Cartesian frame $\{o; \mathbf{e}_1, \mathbf{e}_2\}$; for x a point in $\mathcal{B}$, let us denote by $\mathbf{x} = x - o = x_\alpha \mathbf{e}_\alpha$ its position vector with respect to the origin o. We assume that each material point is endowed with a fiber, whose local direction is $\mathbf{n}(\vartheta) = \cos\vartheta \mathbf{e}_1 + \sin\vartheta \mathbf{e}_2$.

Following [11, 23, 29, 24, 25], we consider ϑ an *internal state variable*, which influences the free energy and whose rate of change is governed by an evolution law, in which the strain appears; within this framework, the dissipation rests upon the evolution of ϑ.

A thermodynamic process for $\mathcal{B}$ is described by a list of functions of x and the time t, that we fix as $\Lambda = \{\mathbf{E}, \vartheta\}$, where $\mathbf{E} = \operatorname{sym} \nabla \mathbf{u}$ is the linearized strain measure expressed in terms of the displacement field $\mathbf{u}$. We assume that there are no body forces; the mechanical forces acting on the body $\mathcal{B}$ can be then resolved into a symmetric stress tensor $\mathbf{T}$. For sake of simplicity, we confine our attention to a linearized setting for the macroscopic motion, so that there is no need to distinguish between referential and current configurations.

A process for $\mathcal{B}$ is then described by the following fields: (i) the spatial position of a material point in the motion; (ii) the symmetric Cauchy stress tensor $\mathbf{T}$; (iii) the free energy ψ; (iv) the internal variable ϑ. All these fields have to be related to the process by extra *constitutive mappings*, depending on Λ. The material point is then characterized by the response functions

$$\mathbf{T} = \widehat{\mathbf{T}}(\mathbf{E}, \vartheta), \qquad \psi = \widehat{\psi}(\mathbf{E}, \vartheta), \qquad \dot{\vartheta} = g(\mathbf{E}, \vartheta), \tag{1}$$

where $g(\mathbf{E}, \vartheta)$ is the response function which gives $\dot{\vartheta}$ when $\mathbf{E}$ and ϑ are known at each material point. Such a set of functions, defined for all x in $\mathcal{B}$ and all t is a thermodynamic

process in $\mathcal{B}$ if and only if it is compatible with the balance of forces $\mathrm{Div}\,\mathbf{T} = \mathbf{0}$, and then $\mathrm{Div}\,\widehat{\mathbf{T}}(\mathbf{E},\vartheta) = \mathbf{0}$.

The evolution equation $(1)_3$ for ϑ is obtained from a *dissipation principle*. In particular, we require that the rate of the energy dissipation — *i.e.*, the difference between the power expended along a process and the time derivative of the free energy — should be non-negative for all body-parts and at all time

$$\delta = \mathbf{T}\cdot\dot{\mathbf{E}} - \dot{\psi} \geq 0. \tag{2}$$

On taking into account (1), (2) implies

$$\mathbf{T} = \widehat{\mathbf{T}}(\mathbf{E},\vartheta) = \partial_{\mathbf{E}}\widehat{\psi}(\mathbf{E},\vartheta), \tag{3}$$

and the residual *dissipation inequality*

$$\delta = \tau\,\dot{\vartheta} \geq 0, \qquad \tau = \widehat{\tau}(\mathbf{E},\vartheta) = -\partial_{\vartheta}\widehat{\psi}(\mathbf{E},\vartheta) \tag{4}$$

characterizing the energy dissipated during the remodeling; τ is the *torque* associated to the fiber remodeling. We make the basic hypothesis that the remodeling flow incurs dissipation, in the sense that

$$\tau \neq 0 \quad \text{whenever} \quad \dot{\vartheta} \neq 0. \tag{5}$$

As in perfect plasticity, we let the evolution of ϑ depend on a scalar-valued *yield function* $f(\tau, Y)$, where the positive constant $Y > 0$ is the *remodeling flow resistance*:

$$f(\tau, Y) = |\tau| - Y, \tag{6}$$

so that the evolution equation $(1)_3$ becomes the (associative) *flow rule*

$$\dot{\vartheta} = \omega\,\partial_{\tau} f(\tau, \mathbf{E}), \tag{7}$$

with $\omega \in \mathbb{R}$, subject to the Kuhn-Tucker conditions

$$\omega \geq 0, \quad f(\tau, Y) \leq 0, \quad \omega f(\tau, Y) = 0. \tag{8}$$

Correspondingly,

$$\mathcal{E}(Y) = \{\tau \,|\, f(\tau, Y) \leq 0)\}, \qquad \mathcal{Y}(Y) = \{\tau \,|\, f(\tau, Y) = 0\} \tag{9}$$

respectively denote the set of torques in the *elastic range* for a given Y and its boundary, namely the *yield set*. On choosing the yield function as in (6), (7) implies that $\dot{\vartheta} = \omega\,\mathrm{sgn}\tau$ and, as $\omega \geq 0$, the normality rule[1]

$$\mathrm{sgn}\dot{\vartheta} = \mathrm{sgn}\tau. \tag{11}$$

[1]This formulation is based on a maximum dissipation principle (see *e.g.* the Hill's principle in plasticity): the dissipation δ caused by the actual torque τ for a given $\dot{\vartheta}$ results in the maximum possible value for δ over all torques τ^* in the elastic range $\mathcal{E}(Y)$, *i.e.*,

$$\tau\dot{\vartheta} \geq \tau^*\dot{\vartheta}, \quad \forall \tau^* \in \mathcal{E}(Y). \tag{10}$$

Remark 1. *This formulation can be easily rephrased within a variational framework. In particular, the problem at a generic time t_i can be traced back to the search of a local minimum in a suitable space:*

$$\min_{\mathbf{u},\vartheta} \int_{\mathcal{B}} \left(\widehat{\psi}(\mathbf{E}(\mathbf{u}), \vartheta) + Y \int_0^{t_i} |\dot{\vartheta}(\tau)| \mathrm{d}\tau \right), \tag{12}$$

Such a formulation leads to a phase-field model, as in plasticity [42], where the role of the plastic strain is played by the internal variable ϑ.

3. Choice of the free energy and implications on the material response

We assume the response function for the free energy as

$$\psi = \widehat{\psi}(\mathbf{E}, \vartheta) = \frac{1}{2}\mathbb{C}(\mathbf{n}(\vartheta))\mathbf{E} \cdot \mathbf{E}, \tag{13}$$

where $\mathbb{C}\big(\mathbf{n}(\vartheta)\big)$ is the elasticity tensor of a linearly elastic transversely isotropic material, with respect to the direction $\mathbf{n}(\vartheta)$. It is well known that the most general representation for such an elasticity tensor leads to

$$\widehat{\psi}(\mathbf{E}, \vartheta) = \mu|\mathbf{E}|^2 + \frac{\lambda}{2}(\operatorname{tr}\mathbf{E})^2 + c_1(\operatorname{tr}\mathbf{E})\,\mathbf{E}\,\mathbf{n}(\vartheta) \cdot \mathbf{n}(\vartheta) + c_2\,(\mathbf{E}\,\mathbf{n}(\vartheta) \cdot \mathbf{n}(\vartheta))^2, \tag{14}$$

where λ and μ are the Lamé coefficients and c_1 and c_2 the material constants characterizing the transversely isotropic response. In order to ensure that the energy is a positive definite quadratic form, the following conditions must hold true:

$$2\mu + \lambda > 0, \quad \mu > 0, \quad 2(2\mu + \lambda)c_2 > c_1^2 - 4\mu c_1 - 4\mu(\mu + \lambda). \tag{15}$$

We say that the material constants are *admissible* if (15) holds true. For fixed λ and μ, the set $\mathcal{P}$ of constants $(c_1, c_2) \in \mathbb{R}^2$ such that $(15)_{1,2}$ is satisfied is called the admissibility region. This region is then bounded by a parabola and it is shown in gray Fig. 1 (left).

Remark 2. *For sake of simplicity, we decided to limit our attention to a geometrically linear setting, for what concerns the elastic strains. Customarily, soft biological tissues exhibiting this kind of remodeling undergo finite strains. Adopting a more complex energy is of course affordable, but does not change significantly the model. In particular, if we restrict the attention to a linear constitutive relation – such in a Saint-Venant Kirchhoff material – interpreting* $\mathbf{E}$ *in* (14) *as the linearized strain tensor, or as the Green-Lagrangian strain, is rather equivalent, in the homogeneous problem.*

3.1. Elastic response at given fiber direction

Having fixed the fiber direction $\mathbf{n}(\vartheta)$, we now study how the constants c_1 and c_2 affect the anisotropic material response in terms of Young modulus and Poisson ratio. Clearly, all this is well known, see for instance [46], but we find it useful to recall it here along with some new definitions.

In particular, the Young modulus and the Poisson ratio are defined with reference to a uni-axial traction test $\bar{\mathbf{T}} = \sigma\,\mathbf{t} \otimes \mathbf{t}$ where $\mathbf{t} = \cos\alpha\mathbf{e}_1 + \sin\alpha\mathbf{e}_2$ is the testing direction.

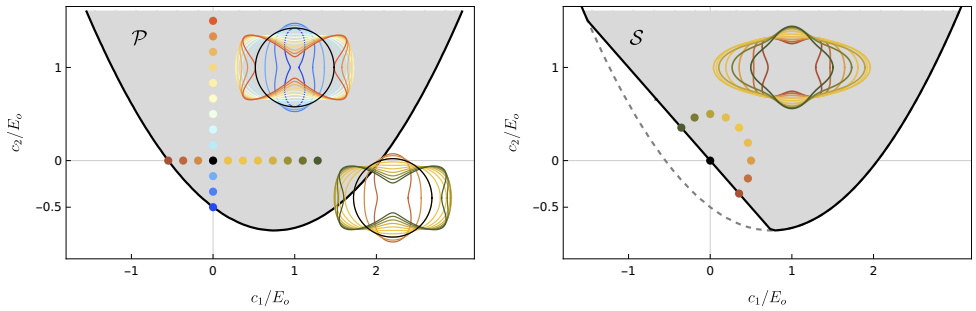

Figure 1: *Left.* The admissibility region $\mathcal{P}$ (in gray) in the plane $(c_1/E_0, c_2/E_0)$ where E_0 is the Young modulus of the isotropic case. The polar plots of the Young modulus, for the two sequences of points within $\mathcal{P}$, show the material stiffening effect due to c_1 and c_2 parameters. *Right.* The region $\mathcal{S}$ of stiffening fibers.

The corresponding strain is $\bar{\mathbf{E}} = \mathbb{C}^{-1}(\mathbf{n}(\vartheta))\bar{\mathbf{T}}$ with the elasticity tensor $\mathbb{C}$ being defined by (14). The Young modulus and Poisson ratio are defined as

$$E(\alpha,\vartheta) = \frac{\bar{\mathbf{T}}\,\mathbf{t}\cdot\mathbf{t}}{\bar{\mathbf{E}}\,\mathbf{t}\cdot\mathbf{t}} = \hat{E}(\alpha-\vartheta), \quad \nu(\alpha,\vartheta) = -\frac{\bar{\mathbf{E}}\,\mathbf{t}^{\perp}\cdot\mathbf{t}^{\perp}}{\bar{\mathbf{E}}\,\mathbf{t}\cdot\mathbf{t}} = \hat{\nu}(\alpha-\vartheta), \tag{16}$$

respectively. They clearly depend only on the difference $(\alpha-\vartheta)$ between the testing and fiber directions and reduce to the standard isotropic expressions when $c_1 = c_2 = 0$. The explicit expressions for the functions $\hat{E}$ and $\hat{\nu}$ are given in the Appendix A. Polar plots of these functions in terms of the angle $(\alpha-\vartheta)$ are meaningful visualizations of the stiffening effects of the constants c_1 and c_2 and are used extensively, see Fig. 1.

Denoting (E_f, ν_f) and $(E_f^{\perp}, \nu_f^{\perp})$ the Young modulus and the Poisson ratio in the directions parallel $(\alpha = \vartheta)$ and orthogonal $(\alpha = \vartheta - \pi/2)$ to the fiber, we have respectively[2]

$$\begin{aligned} E_f &= \frac{4\mu(c_2+\mu+\lambda)+4c_1\mu+2c_2\lambda-c_1^2}{2\mu+\lambda}, \qquad \nu_f = \frac{c_1+\lambda}{2\mu+\lambda}, \\ E_f^{\perp} &= \frac{4\mu(c_2+\mu+\lambda)+4c_1\mu+2c_2\lambda-c_1^2}{2\mu+\lambda+2(c_1+c_2)}, \qquad \nu_f^{\perp} = \frac{c_1+\lambda}{2\mu+\lambda+2(c_1+c_2)}. \end{aligned} \tag{17}$$

We say that *a fiber is stiffening* whenever the ratio

$$\frac{E_f}{E_f^{\perp}} = 1 + \frac{2(c_1+c_2)}{2\mu+\lambda} \tag{18}$$

is greater than 1; since $(15)_1$ has to be satisfied, the set of all stiffening fibers $\mathcal{S}$ is, therefore,

$$\mathcal{S} = \{(c_1,c_2) \in \mathcal{P}, c_1+c_2 > 0\}, \tag{19}$$

and it is shown in Fig. 1 on the right.

[2]From (15), we notice that the Poisson ratio ν_f is not bounded.

3.2. The elastic range

In this section we characterize the elastic range in terms of the strain. Since the remodeling torque has not reached the critical threshold, $\mathcal{E}(Y)$ can be regarded as the set of strains for which the fiber direction ϑ cannot evolve (*cf.* (6) and (7)), and the material response is purely elastic.

With (14), labeling $\mathbf{n}^\perp(\vartheta) = \partial_\vartheta \mathbf{n}(\vartheta) = -\sin\vartheta \mathbf{e}_1 + \cos\vartheta \mathbf{e}_2$, the remodeling torque is

$$\begin{aligned}\tau(\mathbf{E},\vartheta) = -\partial_{\mathbf{n}}\widehat{\psi}(\mathbf{E},\mathbf{n}(\vartheta))\cdot\partial_\vartheta\mathbf{n}(\vartheta) = -2\big(c_1 \mathrm{tr}\,\mathbf{E} + 2\,c_2\,\mathbf{E}\mathbf{n}(\vartheta)\cdot\mathbf{n}(\vartheta)\big)\,\mathbf{E}\mathbf{n}(\vartheta)\cdot\mathbf{n}^\perp(\vartheta) = \\ = -\big((c_1+c_2)(E_{11}+E_{22}) + c_2(E_{11}-E_{22})\cos 2\vartheta + 2c_2E_{12}\sin 2\vartheta\big)\times \\ \times\big(2E_{12}\cos 2\vartheta + (E_{22}-E_{11})\sin 2\vartheta\big).\end{aligned} \tag{20}$$

where $E_{ij} = \mathbf{E}\cdot\mathbf{e}_i\otimes\mathbf{e}_j$, $(i,j=1,2)$, and the elastic range can be explicitly expressed in terms of the strain $\mathbf{E}$, the only visible state variable:

$$\mathcal{E}(Y) = \{\mathbf{E}\in \mathrm{Sym},\ \sup_{-\pi/2\le\vartheta\le+\pi/2}|\widehat{\tau}(\mathbf{E},\vartheta)| \le Y\}. \tag{21}$$

Without loss of generality, we use a spectral decomposition of the deformation

$$\mathbf{E} = \varepsilon_1\,\mathbf{a}\otimes\mathbf{a} + \varepsilon_2\,\mathbf{a}^\perp\otimes\mathbf{a}^\perp,$$

where $\varepsilon_1 \ge \varepsilon_2$ and $\mathbf{a}$, $\mathbf{a}^\perp$ are two orthogonal unit vectors. Substituting in (20), the elastic range $\mathcal{E}(Y)$ simplifies into the set of deformations such that

$$\sup_{0\le\varphi\le\pi}|(2\,(c_1+c_2)\,\varepsilon_c + c_2R\cos 2\varphi)\,\sin 2\varphi| \le Y/R, \tag{22}$$

with $R = \varepsilon_1 - \varepsilon_2 \ge 0$, $\varepsilon_c = (\varepsilon_1+\varepsilon_2)/2$ the radius and the center of the Mohr's circle corresponding to $\mathbf{E}$ and $\cos\varphi = \mathbf{a}\cdot\mathbf{n}$. Assuming $c_2R \neq 0$, the sup condition can be easily solved in terms of $\tan\varphi$ and the ratio $r = 2(c_1+c_2)\varepsilon_c/(c_2R)$. Its solution reads

$$h(r) = \sup_{0\le\varphi\le\pi}|(r+\cos 2\varphi)\,\sin 2\varphi| \le \frac{Y}{|c_2|R^2}, \tag{23}$$

where the dimensionless function $h(r)$ is found to be

$$h(r) = \frac{\sqrt{r^2+8}+3|r|}{16}\sqrt{2|r|\left(\sqrt{r^2+8}-|r|\right)+8}, \tag{24}$$

plotted in Fig. 2 on the left. When r is small, say for instance $(c_1+c_2)\to 0$, we have $h(r\to 0) = 1/2$ and the elastic range (21) reduces essentially to limit the maximal shear deformation: $R^2 \le 2Y/|c_2|$. Instead, for large r, say for instance $c_2\to 0$, we have $h(r\to\infty) = |r|$ and the elastic range (21) reduces to a far less common condition, namely $R|\varepsilon_c| \le Y/(2|c_1+c_2|)$, where the product of the radius and center of the Mohr's circle is bounded.

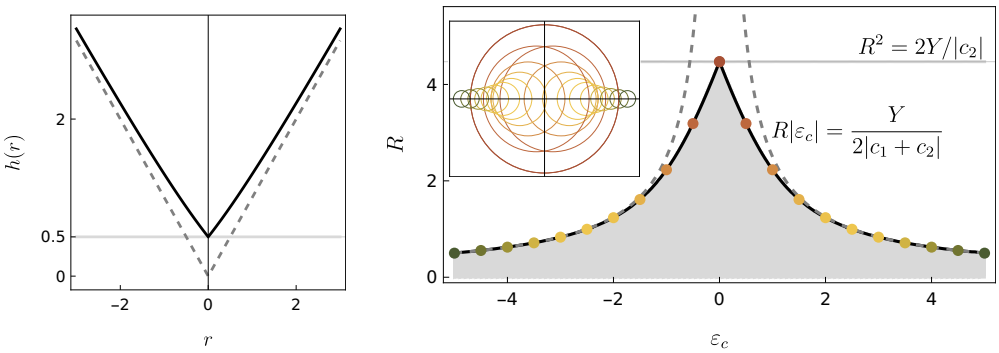

Figure 2: *Left.* The function $h(r)$ defined in (24); the gray dashed lines indicate to the plot of $|r|$. *Right.* The elastic range $\mathcal{E}(Y)$ in the plane (ε_c, R) for $c_1 = c_2 = 0.1$. The top left inset shows a sequence of Mohr's circles on the yield set.

4. The traction problem

We examine the traction problem sketched in Fig. 3. A rectangular sample, of length L and height H, is left free on the upper and lower sides and clamped on the left side; the horizontal displacement of the points on the right side is imposed to be $\mathbf{u} = \varepsilon L \mathbf{e}_1$ whilst their vertical displacement is left free. The material is homogeneous: the initial fiber orientation[3] is $\vartheta_0 \in [0, \pi/2]$. We study the solution, in terms of strain and fiber rotation, as the imposed displacement εL monotonically increases starting from 0.

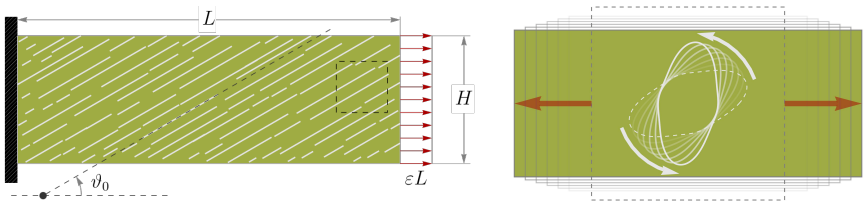

Figure 3: *Left.* The traction problem of a rectangular sample: ϑ_0 is the initial direction for all the fibers. *Right.* Local behavior of a stiffening material under traction.

In our set-up the strain field is not allowed to be homogeneous. Indeed, assuming a non-vanishing Poisson effect, the horizontal stretch is associated to a contraction in the vertical direction; near the left side this contraction is impeded by the clamp condition. However, the Saint-Venant principle [21] suggests that, sufficiently far from left side, a homogeneous strain field is possible, despite its stability outside the elastic range is not guaranteed.

Hence, in the next section, we study and find a complete analytical characterization of the homogeneous case, where both the strain $\mathbf{E}$ and the fiber rotation ϑ are uniform in space. Its interest will be relevant beyond the particular set-up chosen for the material and the boundary conditions.

[3] It suffices to consider $\vartheta_0 \in [0, \pi/2]$ as $\vartheta_0 \equiv \vartheta_0 + \pi$ and, for the symmetry of the problem, $\vartheta_0 \equiv -\vartheta_0$.

4.1. The homogeneous solution (far from the clamped side)

All the relevant fields (strains, stresses, fiber rotations and remodeling torques) are assumed uniform in space. Hence $E_{11} = \varepsilon$ and the boundary conditions on the up and bottom sides, namely $T_{22} = T_{12} = 0$, are used to determine E_{12} and E_{22}, see the expressions in Appendix B. Using the constitutive relation and $(20)_2$, also the stress $T_{11} = \widetilde{T}_{11}(\varepsilon, \vartheta)$, the elastic energy $\psi = \widetilde{\psi}(\varepsilon, \vartheta)$ and the remodeling torque

$$\tau(\varepsilon, \vartheta) = \frac{C_3 \left(\cos 2\vartheta \left(2c_2(\lambda+\mu) - c_1^2\right) + 2\mu(c_1+c_2)\right) \sin 2\vartheta}{\left(\cos 4\vartheta \left(c_1^2 - 2c_2(\lambda+\mu)\right) - c_1^2 - 8\mu(c_1+c_2)\cos 2\vartheta + C_4\right)^2} \varepsilon^2, \tag{25}$$

are determined in terms of ε. Here C_3 and C_4 are combinations of the material parameters only: the interested reader can find the explicit expressions of C_3, C_4, T_{11} in Appendix B.

To completely solve the problem, it remains to compute $\vartheta = \hat{\vartheta}(\varepsilon)$ for $\varepsilon \in [0, \infty)$ using (7). Here, the yield set $\mathcal{Y}$ is implicitly given by the lowest strain value $\bar{\varepsilon}$ such that $|\tau(\bar{\varepsilon}, \vartheta_0)| = Y$. For $\varepsilon \leq \bar{\varepsilon}$, *i.e.* in the elastic range, the fiber orientation cannot evolve:

$$\hat{\vartheta}(\varepsilon) = \vartheta_0, \qquad \text{for } 0 \leq \varepsilon < \bar{\varepsilon}.$$

For $\varepsilon \geq \bar{\varepsilon}$, the fiber orientation must evolve in order to remain at equilibrium; thus $\hat{\vartheta}(\varepsilon)$ is implicitly defined by:

$$\tau(\varepsilon, \hat{\vartheta}(\varepsilon)) = \pm Y, \qquad \text{for } \varepsilon \geq \bar{\varepsilon},$$

the correct branch being determined by the normality rule (11).

To establish the stability of these equilibrium branches at each given level of strain, it is sufficient to check whether they correspond to minima of the elastic energy, namely

$$\partial^2_{\vartheta^2} \widetilde{\psi}(\varepsilon, \vartheta) \equiv -\partial_\vartheta \tau(\varepsilon, \vartheta) > 0. \tag{26}$$

Notice that $\widetilde{\psi}(\varepsilon, \cdot)$ can serve as a Lyapunov function for the evolution equation $\dot{\vartheta} = g(\varepsilon, \vartheta)$ since $\partial_\vartheta \widetilde{\psi}(\varepsilon, \vartheta)\, g(\varepsilon, \vartheta) \leq 0$ due to (4). Therefore any stable equilibrium point, according to (26), is Lyapunov-stable.

Finally, the asymptotic values of the fiber orientation for $\varepsilon \to \infty$ are found as the roots of the function $\gamma(\vartheta) = \tau(\varepsilon, \vartheta)/\varepsilon^2$ *i.e.* when the remodeling torque vanish disregarding of the actual strain value. Inspecting (25) we see that $\gamma(\vartheta)$ can vanish for $\vartheta = 0$, $\vartheta = \pi/2$ and

$$\vartheta_\infty = \frac{1}{2} \arccos\left(\frac{2\mu(c_1+c_2)}{c_1^2 - 2c_2(\mu+\lambda)}\right), \tag{27}$$

which is real only if the argument of the arccos function is bounded in modulus by 1. This circumstance leads to classify the *stiffening* materials defined in (19), into the following three classes:

$$\text{A)} -2\mu(c_1+c_2) > c_1^2 - 2c_2(\mu+\lambda), \qquad \exists\, \vartheta_\infty \in \mathbb{R},\ \vartheta_\infty \text{ is a minimum of } \psi, \tag{28}$$

$$\text{B)} -2\mu(c_1+c_2) < c_1^2 - 2c_2(\mu+\lambda) < 2\mu(c_1+c_2), \quad \nexists\, \vartheta_\infty \in \mathbb{R}, \tag{29}$$

$$\text{C)}\ c_1^2 - 2c_2(\mu+\lambda) > 2\mu(c_1+c_2), \qquad \exists\, \vartheta_\infty \in \mathbb{R},\ \vartheta_\infty \text{ is a maximum of } \psi. \tag{30}$$

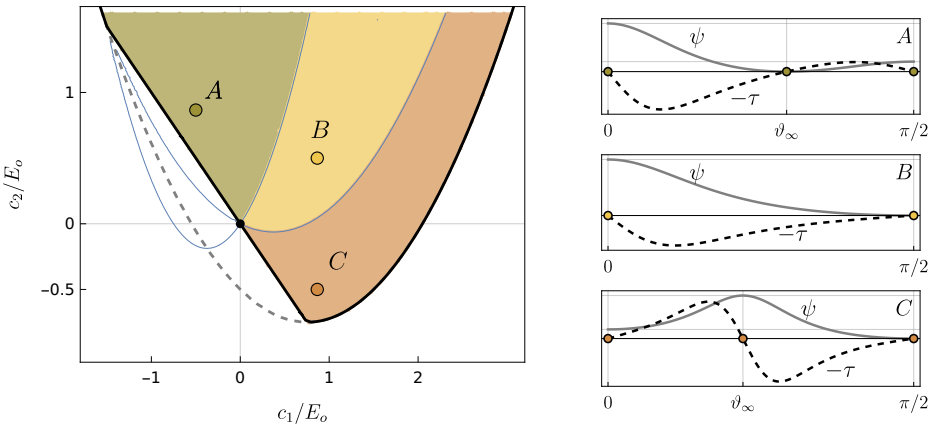

Figure 4: *Left.* Three types of stiffening materials are possible. *Right.* The graphs of ψ (gray) and $\partial_\vartheta \psi = -\tau$ (dashed) when (c_1, c_2) are chosen as the points in the regions A, B, C on the left.

These regions are plotted on the left in Fig. 4. In the same figure on the right the elastic energy ψ (gray) and the its derivative (*i.e.*, the opposite of remodeling torque τ) (dashed) are plotted against the fiber orientation for three materials in the regions A, B, and C.

For materials in the class A, there is one minimum $0 \leq \vartheta_\infty \leq \pi/2$ and two maxima $\vartheta = 0, \pi/2$ of the elastic energy (Fig. 4 top right). The evolution of the homogeneous traction problem is depicted in Fig. 5 on the left by means of sequences of gray arrows. Starting from $0 < \vartheta = \vartheta_0 < \pi/2$, first the yield set is reached and then the fiber rotates; if the yield set is reached in an unstable branch (dashed), $\vartheta(\varepsilon)$ suffers a jump to reach the stable branch and then smoothly tends to ϑ_∞ in (27). Note that for such materials, apart from the unstable situations of perfectly horizontal and vertical fibers, any initial fiber orientation ϑ_0 will asymptotically tend to ϑ_∞. If $\vartheta_0 < \vartheta_\infty$ the rotation $\dot{\vartheta}$ is positive as in Fig. 3 right; otherwise the fibers rotate clockwise.

For materials in the class B, $\vartheta = \pi/2$ is the only minimum, while $\vartheta = 0$ is a maximum of the elastic energy (Fig. 4 center right). Again the evolution of the homogeous traction problem is depicted in Fig. 5 center by means of sequences of gray arrows. Here, apart when starting from horizontal fibers, the rotation can be discontinuous or continuous but is always positive (counterclockwise): asymptotically all the fibers tend to dispose vertically.

Finally, for materials in the class C, ϑ_∞ exists but it is a maximum while $\vartheta = 0, \pi/2$ are minima of the elastic energy (Fig. 4 bottom right). Hence, as shown in Fig. 5 right, any fiber which is initially lower than ϑ_∞ will rotate clockwise up to $\vartheta = 0$; viceversa any initial orientation greater than ϑ_∞ will rotate counterclockwise and tend to dispose vertically. This case is particularly interesting and calls for the analysis of an initial random distribution of orientations where the fibers, violating the hypothesis of homogeneity, will possibly segregate into two phases.

Remark 3. *A stiffening material can exhibit a negative Poisson ratio, for some choice of* (c_1, c_2, ϑ_0)*. For instance , the material A in Fig. 4 if the initial orientation is sufficiently low* $(0 < \vartheta_0 \lesssim 15°)$ *is auxetic having* $\nu \simeq -0.1$*. However, under traction, the evolution of* ϑ *follows the gray sequence of arrows on the left of Fig. 5:* ϑ *starts at* $\vartheta_0 \simeq 6°$ *suffers a*

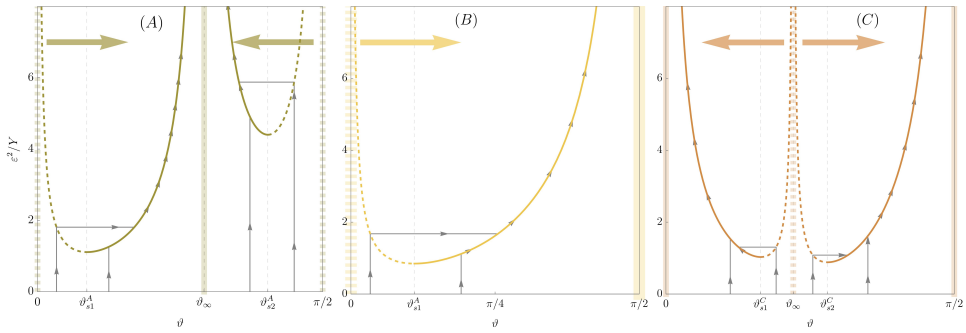

Figure 5: The yield sets $|\tau(\varepsilon, \vartheta)| = Y$ in the plane $(\vartheta, \varepsilon^2/Y)$ for the three materials chosen in Fig. 4: the unstable branches are dashed. For each case we show different evolution paths (in gray with arrows) for different values of the initial fiber orientation ϑ_0.

jump of almost $+25°$ *and then evolves continuously toward* $\vartheta_\infty \simeq 53°$. *The corresponding values of the Poisson ratio are plotted in Fig. 6, its asymptotic value being around* 0.2. *Since the plastic remodeling changes the material response, this example shows that, in principle, it is possible to achieve a permanent transition from auxetic to non-auxetic materials (and viceversa) by simply applying mechanical loads .*

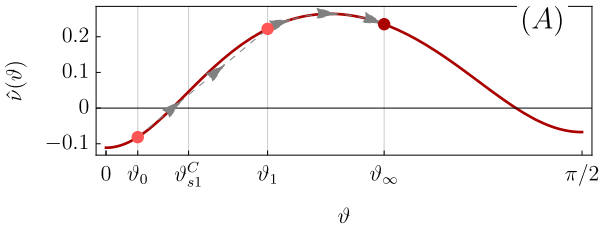

Figure 6: Transition from auxetic to non-auxetic behavior, for the material A in Fig. 4 starting from $\vartheta_0 \simeq 6°$.

4.2. Numerical solution of the non-homogeneous traction problem

As already discussed, the traction problem, see Fig. 3 left, is necessarily non homogeneous and calls for a numerical solution. To this aim we have used an incremental energy minimization framework [44] where the imposed displacement ε is discretized in steps and the total energy (elastic energy and remodeling dissipation) is minimized with respect to the displacement $\mathbf{u}$ and fiber orientation fields ϑ. Specifically, an alternate minimization strategy has been adopted: at each step a sequence of minimizations with respect to $\mathbf{u}$ at fixed ϑ and minimizations with respect to ϑ at a fixed $\mathbf{u}$ is performed until convergence. While the former requires to solve a linear elasticity problem, the latter demands the solution of a nonlinear problem (a modified Newton-Raphson scheme is used). Nevertheless, the minimization in ϑ has the advantage to be local in space and, therefore, effectively parallelizable. The domain has been discretized with an unstructured mesh. The displacement field has been taken in a piece-wise affine finite element space CG1 (continuous Galerkin-grade 1) [10]) over the domain. Instead, the fiber rotational

field, due to the intrinsic locality is projected onto a discontinuous finite element space DG0 (discontinuous Galerkin-grade 0). The time has been discretized with non-uniform steps. The code has been written in `python` as interface to `FEniCS`, a popular open-source computing platform for solving partial differential equations [40, 1]. In particular the package `DOLFIN` [41], a library aimed at automating solution of PDEs using the finite element method, has been used extensively.

The Lamé constants are chosen $\lambda = \mu = 3/8$ in order to have a unitary Young modulus $E_0 = 1$ and $\nu_0 = 1/3$. The anisotropic parameters $c_1 = 0$ and $c_2 = 0.2$ are chosen in the region A: hence, the asymptotic value (27) exists, $\vartheta_\infty \simeq 60°$, and it is a minimum of the elastic energy in the homogeneous case. The initial fiber orientation is uniform and equals $\vartheta_0 = 67.5°$. Since $\vartheta_0 > \vartheta_\infty$, at least far from the clamped side, we expect the fibers to rotate 7.5° counterclockwise to reach the 60° orientation from above.

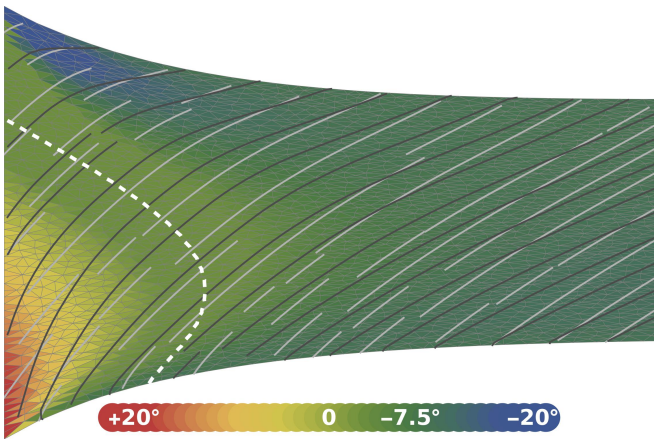

Figure 7: Distribution of the asymptotic fiber rotation, namely $\vartheta(\varepsilon \to \infty) - \vartheta_0$, on the deformed configuration of the traction problem. The initial fibers are marked in light gray, the final in dark gray. In the color legend positive degrees means counterclockwise rotations.

Figure 7 shows the asymptotic distribution of fiber rotations starting from ϑ_0 over the deformed configuration of the sample. Note that already at a distance $\simeq H$ from the left side the solution is almost homogeneous and coincide with the analytical predictions of Sec. 4.1. The white dashed curve indicates the locus where ϑ has not evolved; indeed the presence of shear near the clamp alters the fiber orientation value at which the remodeling torque vanishes. The shear strains are also responsible for the two zones, respectively red and blue, where the asymptotic rotation is sensibly bigger and lower than $-7.5°$.

5. Conclusions and perspectives

We have presented a simple model of fibrous materials that may undergo an internal reorganization, which turns out in a plastic change of the orientation angle of the fibers, if a threshold is achieved. In particular, we have proposed an analytical description of the elastic range and the yield set, we analytically determined the solution of the evolution problem in the homogeneous case and proposed some numerical results for a non-homogeneous condition.

The model assumes that the material is homogeneous, so that each material point is endowed with an additional kinematical descriptor, representing the fiber direction, to be intended as a proper statistical mean of the fiber directions in a sufficiently small neighborhood of that point. We have also considered that the fibers are sparsely dispersed, so that there is not any direct interaction between them. Although the macroscopic displacement is assumed small, and a linear strain measure has been adopted, there is no limitation on the rotation of the fibers. Within these assumptions, we have considered the most general energy accounting for the anisotropy induced by the fibers.

In our present model, we have focused on the plastic-like threshold mechanism and we have neglected other possible sources of dissipation, such as those coming from viscous effects. A first generalization that we will present in a forthcoming work includes rate-dependent effects. As an outcome, it can be expected that the non-regular evolution that our model encompasses (see the jumps in Fig. 5) becomes more realistically smooth, so that the asymptotic behavior that we were able to analytically describe, could be reached in a characteristic time, depending on the viscosity.

Another interesting point that we postpone to a future specific analysis concerns a deeper investigation on type C materials (see Fig. 4): in this case the energy exhibits a double-well landscape which may induce a phase transition phenomenon, with eventually segregation. This circumstance is indeed detected in some experiments involving fibrous biological materials [27]. A deeper insight for these kind of materials demands, moreover, for the possibility that the anisotropic constants c_1 and c_2 be allowed to evolve, in order to mimic the tendency to stiffen the matrix when new fibers are generated during the remodeling process.

Acknowledgments

AF is supported by the Project PRIN2017 #20177TTP3S. SV is supported by the Project PRIN2017 #20173C478N.

Appendix A. Young modulus and Poisson ratio at given ϑ

The explicit expressions for the quantities defined in Sec. 3.1 are here reported. Specifically, with ϑ the fiber direction and α the direction of the uni-axial traction test, $(16)_1$ and $(16)_2$ are respectively:

$$\hat{E}(\alpha-\vartheta) = 8\mu\left(-c_1^2+4c_1\mu+4\mu(c_2+\lambda+\mu)+2c_2\lambda\right)\times \\ \Big(\cos(4(\alpha-\vartheta))\left(c_1^2-2c_2(\lambda+\mu)\right)-c_1^2-8\mu(c_1+c_2)\cos(2(\alpha-\vartheta))+ \\ 8c_1\mu+2c_2(\lambda+5\mu)+8\mu(\lambda+2\mu)\Big)^{-1}, \quad \text{(A.1)}$$

and

$$\hat{\nu}(\alpha-\vartheta) = \Big(\cos(4(\alpha-\vartheta))\left(c_1^2-2c_2(\lambda+\mu)\right)-c_1^2+8c_1\mu+2c_2(\lambda+\mu)+8\lambda\mu\Big)\times \\ \Big(\cos(4(\alpha-\vartheta))\left(c_1^2-2c_2(\lambda+\mu)\right)-8\mu(c_1+c_2)\cos(2(\alpha-\vartheta))-c_1^2+8c_1\mu+ \\ 2c_2(\lambda+5\mu)+8\mu(\lambda+2\mu)\Big)^{-1}. \quad \text{(A.2)}$$

Appendix B. Strain and stress in the homogeneous case

The explicit expressions used in Sec.4.1 for the strains

$$\begin{aligned} E_{22} &= \frac{c_1^2 - 8c_1\mu - 8\lambda\mu - 2c_2(\mu+\lambda) - (c_1^2 - 2c_2(\mu+\lambda))\cos 4\vartheta}{8\Big(\big(2c_1\mu - (c_1^2 - 2c_2\lambda)\cos^2\vartheta\big)\sin^2\vartheta + 2c_2\mu\sin^4\vartheta + \mu(2\mu+\lambda+c_2\sin^2 2\vartheta)\Big)}\,\varepsilon, \\ E_{12} &= \frac{\Big(\big(c_1^2 - 2c_2(\mu+\lambda)\big)\cos 2\vartheta - 2\mu(c_1+c_2)\Big)\sin 2\vartheta}{(2\mu+\lambda)\big(4\mu + c_2(1-\cos 4\vartheta)\big) - 2c_1(c_1 - 4\mu + c_1\cos 2\vartheta)\sin^2\vartheta + 8c_2\mu\sin^4\vartheta}\,\varepsilon, \end{aligned} \tag{B.1}$$

the only non-vanishing stress component T_{11}

$$T_{11} = \frac{4\mu\left(2c_2(\lambda+2\mu) + 4c_1\mu - c_1^2 + 4\mu(\lambda+\mu)\right)}{4c_2\sin^2\vartheta\cos 2\vartheta(\lambda+\mu) + \lambda + 3\mu) + 8c_1\mu\sin^2\vartheta - c_1^2\sin^2(2\vartheta) + 4\mu(\lambda+2\mu)}\,\varepsilon \tag{B.2}$$

and the constants

$$C_3 = 32\mu\left(4c_1\mu - c_1^2 + 4\mu(c_2+\lambda+\mu) + 2c_2\lambda\right),\ C_4 = 8c_1\mu + 2c_2(\lambda+5\mu) + 8\mu(\lambda+2\mu), \tag{B.3}$$

introduced in (25).

References

[1] Aln, M. S., Kehlet, B., Logg, A., Richardson, C., Ring, J., Rognes, E., Wells, G. N., 2015. The FEniCS Project Version 1.5, 15.

[2] Andrianov, I. V., Danishevs'kyy, V. V., Weichert, D., 2002. Asymptotic determination of effective elastic properties of composite materials with fibrous square-shaped inclusions. European Journal of Mechanics - A/Solids 21 (6), 1019–1036.

[3] Baaijens, F., Bouten, C., Driessen, N. Modeling collagen remodeling, Journal of Biomechanics Volume 43, 1, 2010, 166-175

[4] Ban, E., Franklin, J. M., Nam, S., Smith, L., Wang, H., Wells, R., Chaudhuri, O., Liphardt, J., Shenoy, V., 2018. Mechanisms of plastic deformation in collagen networks induced by cellular forces. Biophysical Journal 114 (2), 450–461.

[5] Barthelat, F., Yin, Z., Buehler, M., 2016. Structure and mechanics of interfaces in biological materials. Nat. Rev. Mater. 1 (16007).

[6] Bosco, E., Peerlings, R., Geers, M., 2018. Scale effects in the hygro-thermo-mechanical response of fibrous networks. European Journal of Mechanics - A/Solids 71, 113–121.

[7] Buchmann, B., Engelbrecht, L., Fernandez, P., et al., 2021. Mechanical plasticity of collagen directs branch elongation in human mammary gland organoids. Nat .Commun. 12 (2759).

[8] Chaudhuri, O., Gu, L., Klumpers, D., et al., 2016. Hydrogels with tunable stress relaxation regulate stem cell fate and activity. Nature Mater. 15, 326–334.

[9] Chaudhuri, O., Gu, L., M. Darnell, e. a., 2015. Substrate stress relaxation regulates cell spreading. Nat. Commun. 6 (6365).

[10] Cockburn, B., Fu, G., 2017. A systematic construction of finite element commuting exact sequences. SIAM journal on numerical analysis 55, 1650–1688.

[11] Coleman, B., Gurtin, M., 1967. Thermodynamics with internal state variables. The Journal of Chemical Physics 47 (2), 597–613.

[12] Crevacore, E., Di Stefano, S., Grillo, A. (2019) Coupling among deformation, fluid flow, structural reorganisation and fibre reorientation in fibre-reinforced, transversely isotropic biological tissues, International Journal of Non-Linear Mechanics 111, 1-13

[13] de Gennes, P., Prost, J., 1995. Biology of fibrous composites: development beyond the cell membrane. Clarendon Press.

[14] Discher, D., Janmey, P., Wang, Y., 2005. Tissue cells feel and respond to the stiffness of their substrate. Science 310 (5751), 1139–1143.

[15] Driessen, N.J., Wilson, W., Bouten, C.V., Baaijens, F.P. A computational model for collagen fibre remodelling in the arterial wall. J Theor Biol. 2004 Jan 7;226(1):53-64.

[16] Driessen, N.J.B., Cox, M.A.J., Bouten, C.V.C. et al. Remodelling of the angular collagen fiber distribution in cardiovascular tissues. Biomech Model Mechanobiol 7, 93 (2008).
[17] Dunlop, J. W., Weinkamer, R., Fratzl, P., 2011. Artful interfaces within biological materials. Materials Today 14 (3), 70–78.
[18] Engler, A., Sen, S., Sweeney, H., Discher, D., 2006. Matrix elasticity directs stem cell lineage specification. Cell 126 (4), 677–689.
[19] Ericksen, J., 1991. Introduction to the Thermodynamics of Solids. Chapman & Hall.
[20] Fantner, G., Hassenkam, T., Kindt, J., et al., 2005. Sacrificial bonds and hidden length dissipate energy as mineralized fibrils separate during bone fracture. Nature Mater. 4, 612–616.
[21] Fichera, G., 1979. Remarks on Saint-Venant's principle. Rendiconti di Matematica e delle sue Applicazioni 6 (12 (2)), 181–200.
[22] Gao, H., Ji, B., Jäger, I., Arzt, E., Fratzl, P., 2003. Materials become insensitive to flaws at nanoscale: Lessons from nature. Proceedings of the National Academy of Sciences of the United States of America 100 (10), 5597–5600.
[23] Germain, P., 1973. The method of virtual power in continuum mechanics. Part 2: Microstructure. SIAM Journal on Applied Mathematics 25 (3), 556–575.
[24] Germain, P., 1982. Sur certaines définitions liées à l'énergie en mécanique des solides. International Journal of Engineering Science 20 (2), 245–259.
[25] Germain, P., Nguyen, Q., Suquet, P., 1983. Continuum thermodynamics. Journal of Applied Mechanics 50, 1010–1020.
[26] Godinho, P. M. J., Jajcinovic, M., Wagner, L., Vass, V., Fischer, W. J., Bader, T. K., Hirn, U., Bauer, W., Eberhardsteiner, J., Hellmich, C., 2019. A continuum micromechanics approach to the elasticity and strength of planar fiber networks: Theory and application to paper sheets. European Journal of Mechanics - A/Solids 75, 516–531.
[27] Grekas, G., Proestaki, M., Rosakis, P., J., N., Makridakis, C., Ravichandran, G., 2021. Cells exploit a phase transition to mechanically remodel the fibrous extracellular matrix. J. R. Soc. Interface 18 (20200823).
[28] Grytz, R., Meschke, G. A computational remodeling approach to predict the physiological architecture of the collagen fibril network in corneo-scleral shells. Biomech Model Mechanobiol 9, 225?235 (2010).
[29] Halphen, B., Nguyen, Q., 1975. Sur les matériaux standards généralisés. Journal de Mécanique 14 (1), 39–63.
[30] Hariton, I., deBotton, G., Gasser, T.C. et al. Stress-driven collagen fiber remodeling in arterial walls. Biomech. Model. Mechanobiol. 6, 163-175 (2007).
[31] Himpel, G., Menzel, A., Kuhl, E. and Steinmann, P. (2008), Time-dependent fibre reorientation of transversely isotropic continua – Finite element formulation and consistent linearization. Int. J. Numer. Meth. Engng., 73: 1413-1433.
[32] Humphrey, J.D., Eberth, J.F., Dye, W.W., Gleason, R.L., Fundamental role of axial stress in compensatory adaptations by arteries, Journal of Biomechanics 42, 1, 2009, 1-8.
[33] Irons L, Humphrey JD (2020) Cell signaling model for arterial mechanobiology. PLoS Comput Biol 16(8): e1008161.
[34] Keckes, J., Burgert, I., Frühmann, K., et al., 2003. Cell-wall recovery after irreversible deformation of wood. Nature Mater. 2, 810–813.
[35] Kundler, I., Finkelmann, H., 1995. Strain-induced director reorientation in nematic liquid single crystal elastomers. Macromolecular Rapid Communications 16 (9), 679–686.
[36] Kundler, I., Finkelmann, H., 1998. Director reorientation via stripe-domains in nematic elastomers: influence of cross-link density, anisotropy of the network and smectic clusters. Macromolecular Chemistry and Physics 199 (4), 677–686.
[37] Kurimoto, R., Niiyama, E., Ebara, M., 2016. Fibrous materials. In: Ebara, M. (Ed.), Biomaterials Nanoarchitectonics. William Andrew Publishing, pp. 267–278.
[38] Ling, S., Kaplan, D., Buehler, M., 2018. Nanofibrils in nature and materials engineering. Nature Reviews Materials 3.
[39] Liu, Z., Zhang, Y., Zhang, M., Tan, G., Zhu, Y., Zhang, Z., Ritchie, R. O., 2019. Adaptive structural reorientation: Developing extraordinary mechanical properties by constrained flexibility in natural materials. Acta Biomaterialia 86, 96–108.
[40] Logg, A., Mardal, K.-A., Wells, G. (Eds.), 2012. Automated Solution of Differential Equations by the Finite Element Method. Vol. 84 of Lecture Notes in Computational Science and Engineering. Springer Berlin Heidelberg.
[41] Logg, A., Wells, G. N., Apr 2010. Dolfin. ACM Transactions on Mathematical Software 37 (2),

1–28.
[42] Marigo, J. J., 1989. Constitutive relations in plasticity, damage and fracture mechanics based on a work property. Nuclear Engineering and Design 114 (3), 249–272.
[43] Nagel, T., Kelly, D.J. Remodelling of collagen fibre transition stretch and angular distribution in soft biological tissues and cell-seeded hydrogels. Biomech Model Mechanobiol 11, 325?339 (2012).
[44] Petryk, H., 2003. Incremental energy minimization in dissipative solids. Comptes Rendus Mécanique 331 (7), 469–474.
[45] Sander, E.A., Barocas, V.H. & Tranquillo, R.T. Initial Fiber Alignment Pattern Alters Extracellular Matrix Synthesis in Fibroblast-Populated Fibrin Gel Cruciforms and Correlates with Predicted Tension. Ann Biomed Eng 39, 714-729 (2011).
[46] Spencer, A. J. M., 1984. Constitutive Theory for Strongly Anisotropic Solids. Springer Vienna, Vienna, pp. 1–32.
[47] Studart, A. R., 2013. Biological and bioinspired composites with spatially tunable heterogeneous architectures. Advanced Functional Materials 23 (36), 4423–4436.
[48] Vasios, N., Narang, Y., Akta, B., Howe, R., Bertoldi, K., 2019. Numerical analysis of periodic laminar and fibrous media undergoing a jamming transition. European Journal of Mechanics - A/Solids 75, 322–329.
[49] Wisdom, K., Adebowale, K., Chang, J., et al., 2018. Matrix mechanical plasticity regulates cancer cell migration through confining microenvironments. Nat .Commun. 9 (4144).
[50] Zimmermann, E., Gludovatz, B., Schaible, E., Dave, N., Yang, W., Meyers, M., Ritchie, R., 2013. Mechanical adaptability of the bouligand-type structure in natural dermal armour. Nature Communications 4.